

Logical Majorana zero modes in a nanowire network

Sayandip Dhara,¹ Garry Goldstein,² Claudio Chamon,² and Eduardo R. Mucciolo¹

¹*Department of Physics, University of Central Florida, Orlando, Florida, 32816, USA*

²*Physics Department, Boston University, Boston, Massachusetts 02215, USA*

(Dated: October 17, 2022)

We present a scheme to use physical Majorana quasi-zero modes at each junction of a two-dimensional nanowire network to build a logical Majorana zero mode, the location of which is controllable through gate voltages. The wire-network is a way to realize a proposal by Yang *et al.* [1] to imprint a Kekulé vortex pattern on a honeycomb lattice via gate voltages. We show that a specific type of junction – other than a naive Y- or T-junction – is needed to realize, without breaking time-reversal symmetry, an artificial “graphene” system with Majorana fermions instead of complex ones at each site. The junction we propose (i) traps exactly one physical Majorana (quasi-)zero mode at each site of either a brick wall or honeycomb lattice and (ii) allows this mode to hybridize with all three neighboring sites. Using a lattice of these junctions and starting from an electronic, tight-binding model for the wires, we imprint the voltage patterns corresponding to the Kekulé vortex and observe the emergence of the logical Majorana zero mode at the vortex core. We also provide the range of parameters where this excitation could be realized experimentally.

I. INTRODUCTION

Quantum computation has the potential to solve problems that are intractable in current, classical computers. This potential will be realized when large-scale, fault-tolerant quantum computers become available. In the quest for such machines, two distinct approaches stand out: to increase the number of physical qubits, so that logical qubits can be created and quantum error correction can be applied; [2–4]; or, alternatively, to build qubits that are intrinsically decoherence-resistant due to topological protection [5]. In this paper, we explore the latter but infuse it with elements of the former.

Topological qubits [6–9] based on Majorana zero modes are an example where the qubit has protection against local noise because the information is encoded non-locally, shared between distant localized zero modes. There have been a number of proposals [10–14] in the last decade on how to realize these phases with Majorana zero modes at the endpoints of one-dimensional (1D) wires obtained by interfacing superconducting and semiconducting materials. There has been enormous progress on engineering these material interfaces, as well as on characterizing the properties of the 1D wires and detecting zero-bias peaks at their extremities [15–17]. However, there are still ongoing debates on the exact nature of the zero modes in experimental systems [18], as well as on the proper protocol to separate topological zero-mode states from non-topological Andreev bound states [19, 20].

In this paper, we use 1D wires as building blocks to construct *logical* Majorana zero modes on a two-dimensional (2D) wire network. The location of these logical Majorana zero modes is controlled by applied gate voltages on the wires in the network. The network that we propose builds on that by Yang *et al.* [1], where a hierarchical framework was used to build a logical Majorana zero mode in a two-dimensional (2D) honeycomb network with links consisting of 1D nanowires. The proposal contains three steps. In the first step, each finite-length nanowire in the network is brought to a regime where there is a single Majorana zero mode at each nanowire end. At the vertices of the network, where three nanowires meet,

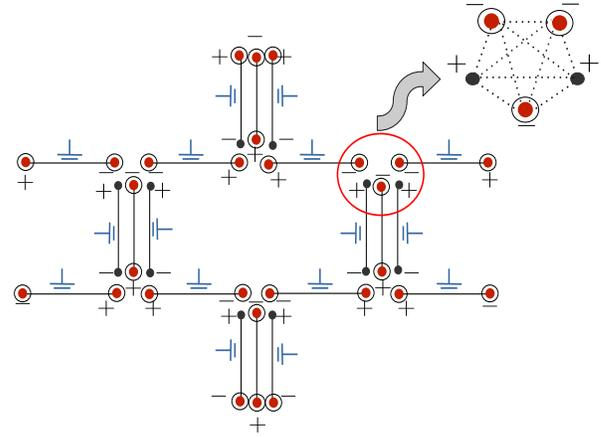


FIG. 1. A unit cell of the brickwall network. Every junction consists of five nanowires and the polarity (\pm signs) correspond to whether the zero mode at a given endpoint of a wire is even or odd under time-reversal symmetry. Notice that the five wires are arranged in such a way that two wires “sister” a (third) central wire in one of the legs of the brickwall lattice. The presence of a nonzero Majorana zero mode amplitude at a nanowire end is indicated by a circular line around a solid circle. The polarities on the nanowires are such that there is only one zero mode per lattice site, and that this mode hybridizes will all the three neighboring sites. The red circle shows a zoom-in of the interwire couplings at a junction.

the Majorana zero modes hybridize. As a result, two of the zero modes are gapped out and only one survives, leaving one Majorana zero mode per vertex. In the second step, by tuning the gate voltages on each wire, these surviving zero modes are made to weakly overlap, creating a band. In the third and final step, a Kekulé vortex modulation [21–23] of gate voltages is employed to open a spectral gap everywhere but on the vortex, which binds a topological zero mode.

Two conditions are essential for obtaining a “Majorana graphene” system on which to build the logical Majorana zero mode at the vortex core: (i) having a single Majorana mode on each site of the honeycomb lattice, and (ii) hybridizing this

mode with all three neighboring sites. In Ref. [1] this was achieved by a fixed pattern of breaking time-reversal symmetry (TRS) at the junction of the three wires connecting at each site. While breaking TRS is not a problem in practice, breaking it in a prescribed pattern on the lattice – in opposite ways in the two sublattices of the honeycomb lattice – could be difficult to achieve. In this paper, we provide a concrete realization of the “Majorana graphene” system of Ref. [1] that requires no breaking of TRS. Here we show that it is impossible, in systems with TRS, to satisfy both conditions (i) and (ii) with junctions of three wires, such as Y- or T-junctions. To satisfy both conditions requires the use of junctions with five wires, where two wires “sister” a third central wire in one of the legs of the Y- or T-junctions, as depicted in Fig. 1.

For systems with TRS, one can define two opposite polarities for the zero modes at the endpoints of a wire, corresponding to whether the zero modes are even (+) or odd (−) under reversal of time. (Which end is assigned + or − depends on the couplings in the Hamiltonian, for example, the sign of the superconductor order parameter, as we discuss in the paper.) The number of zero modes at a junction of $n = n_+ + n_-$ wires, with n_+ of positive and n_- of negative polarity, is given by the integer-valued index $\nu = |n_+ - n_-|$. (The superconducting 1D wires with TRS are in symmetry class BDI [24], which is indexed by a topological invariant $\nu \in \mathbb{Z}$; interactions, which we do not include, break the classification down to \mathbb{Z}_8 [25].) Satisfying the condition (i) above is thus possible with three wires if two have one polarity, and one the other, so that $\nu = |2 - 1| = 1$. However, as we discuss in this paper, the wave function for the zero mode has amplitude only on the *majority* wires, i.e., only on $\rho = \max(n_+, n_-)$ wires (far away from the junction). In the case of junctions of three wires above, the wave function on one site would leak to only $\rho = \max(2, 1) = 2$ out of the three neighbors, yielding a system of decoupled 1D Majorana chains. Therefore it is condition (ii) that poses an obstruction to constructing a 2D system of “Majorana graphene” with Y- or T-junctions. With five-wire junctions as depicted in Fig. 1 we solve the problem with $n_{\pm} = 3$ and $n_{\mp} = 2$ on the two sublattices of the brick-wall lattice, so that $\nu = |3 - 2| = 1$ and $\max(3, 2) = 3$, which satisfy both conditions (i) and (ii).

Using the geometry of Fig. 1, we then construct an electronic tight-binding model of the nanowires and junctions that realize an effective honeycomb lattice of Majorana quasi-zero modes. We implement a Kekulé modulation on the potential of the tight-binding nanowires that opens a bulk spectrum gap, and create vortex that binds a single zero mode to a particular location. Numerical simulations confirm the exact location of the vortex and the ability to move the zero mode around the lattice by a simple change in the gate voltage modulation. To show the presence of a logical Majorana quasi-zero mode, we compute the exact local density of states in the nanowire network in the presence of a vortex. We use our results to estimate the parameters required for an experimental realization and discuss whether the detection of the logical Majorana mode is possible. One of the most important takeaways of this approach of building a logical Majorana zero mode from a collection of physical Majorana quasi-zero modes is that we

can afford less stringent conditions on the physical Majoranas at the nanowire level. The individual nanowires do not need to provide two highly localized zero modes at both ends of the wire; in fact, we exploit the opposite, that in experiments, the nanowire zero modes likely hybridize.

The paper is organized as follows. In Sec. II we present the design rationale for the wire network in Fig. 1. In Sec. III, we discuss a simple model of the 1D quantum wires, and present numerical studies with junctions of three and five wires that support and justify our choice of wire network in Fig. 1, which we then study in Sec. IV, where we introduce the Kekulé modulation of the network to gap the zero modes in the bulk and then demonstrate the gate voltage modulation required to imprint a vortex inside the lattice. In Sec. V we describe the realistic parameters necessary for the experiments. We conclude in Sec. VI with a summary and a discussion of open questions.

II. THE NANOWIRE NETWORK DESIGN RATIONALE

In this section, we justify the design of the nanowire network in Fig. 1. Our goal is to obtain an artificial “Majorana graphene” platform, i.e., a system in which single Majorana (quasi-)zero mode sits on the sites of a brickwall or a honeycomb lattice and hybridizes with the three neighboring sites. This platform shares many of the features of graphene but with Majorana (not complex) fermions on the sites. The programmable hoppings (via gate voltages) allow us to imprint Kekulé vortices in the dimerization pattern, thereby trapping logical Majorana zero modes.

The conditions to realize the “Majorana graphene” platform, namely, (i) that a single (quasi-)zero mode sits on each site, and (ii) that these modes hybridize with the three neighbors, and are connected to two indices that we discuss in this section. Here we shall focus solely on an effective model of Majorana end modes on the nanowires, without diving into any microscopic model of the nanowires or the junctions; that discussion is reserved for the subsequent sections.

Let us start from a single nano wire in a phase in which two Majorana zero modes sit at the wire endpoints, which we label γ_{\pm} . Under the TRS operation \mathcal{T} , one of these modes is even and the other is odd:

$$\mathcal{T} \gamma_{\pm} \mathcal{T}^{-1} = \pm \gamma_{\pm} . \quad (1)$$

The \pm sign associated with the parity of the endpoint zero modes can be thought of as a polarity for that endpoint. Notice that the only possible coupling that can be added to the effective model in which there are only the Majorana endpoints left in the wire is $H = i \gamma_+ \gamma_-$, which is non-local and gaps the wire. That γ_{\pm} have opposite polarity is needed for this H to be both Hermitian and respect TRS.

Consider now a junction where endpoints of multiple wires come together, of which n_+ have positive polarity and n_- have negative polarity, as shown in Fig. 2. The tunneling Hamiltonian H_{junction} is quadratic in γ_{a+} , $a = 1, \dots, n_+$ and γ_{b-} , $b = 1, \dots, n_-$. Moreover, to respect TRS, H_{junction}

$$\mathcal{T} a_l^\dagger \mathcal{T}^{-1} = a_l^\dagger, \quad (10)$$

while a scalar z transforms as

$$\mathcal{T} z \mathcal{T}^{-1} = z^*. \quad (11)$$

Therefore, applying the TRS operation on the chain Hamiltonian we obtain

$$\begin{aligned} \mathcal{T} H_{\text{Kitaev}} \mathcal{T}^{-1} &= \sum_{l=1}^{L-1} \left[-t(a_l^\dagger a_{l+1} + a_{l+1}^\dagger a_l) \right. \\ &\quad \left. + |\Delta| (e^{-i\phi} a_l a_{l+1} + e^{i\phi} a_{l+1}^\dagger a_l^\dagger) \right] \\ &\quad - \mu \sum_{l=1}^L \left(a_l^\dagger a_l - \frac{1}{2} \right). \end{aligned} \quad (12)$$

We can easily verify that in order for the Hamiltonian to be time-reversal symmetric we must have $\phi = \pi n$, where $n = 0, \pm 1, \pm 2, \dots$. In this case, we can write $\Delta = \pm |\Delta|$ (positive or negative). However, since $a_l a_{l+1} = -a_{l+1} a_l$, we can turn a “negative” sign in Δ into a positive one by running the index l from L to 1 instead of 1 to L . Therefore, the orientation of the hopping in the superconductor term and the sign of Δ are related. We can take this into account by classifying time-reversal symmetric Kitaev chain into two classes: “right” and “left”. Thus, in general, for time-reversal symmetric chains we have

$$\begin{aligned} H_{\text{Kitaev}} &= \sum_{l=1}^{L-1} \left[-t(a_l^\dagger a_{l+1} + a_{l+1}^\dagger a_l) \right. \\ &\quad \left. + \eta |\Delta| (a_l a_{l+1} + a_{l+1}^\dagger a_l^\dagger) \right] \\ &\quad - \mu \sum_{l=1}^L \left(a_l^\dagger a_l - \frac{1}{2} \right), \end{aligned} \quad (13)$$

where $\eta = \pm 1$. In fact, we can introduce the concept of chain “polarity”, see Fig. 3, where \pm signs are associated to the endpoints of the chain (i.e, site coordinates $l = 1$ or $l = L$), as well as an arrow, depending on the sign of η . As we showed in Sec. II, the polarity of the chain is connected to how the Majorana zero modes at the chain endpoints ends transform under time reversal.

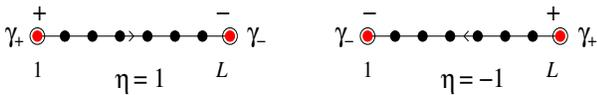


FIG. 3. Schematic illustration of the concept of polarity for time-reversal symmetric Kitaev chains. $\eta = \pm 1$ correspond to whether the Majorana zero modes at the chain endpoints (here indicated by γ_{\pm}) are even/odd or odd/even under time-reversal symmetry.

Although Kitaev’s model describes a platform for the realization of Majorana zero modes in one spatial dimension, electrons have spin and most superconductors occurring in nature have s-wave pairing. More realistic proposals [10, 12, 14] obtain a topological phase and Majorana boundary modes by

including three ingredients: (i) proximitized s-wave superconductivity, (ii) Rashba spin-orbit coupling, and (iii) a Zeeman field.

The continuum Hamiltonian for a single-channel nanowire with electron effective mass m^* , Rashba spin-orbit coupling λ and applied Zeeman field B_z , proximitized with an s-wave superconductor with a pairing amplitude Δ_s , with a chemical potential μ_w can be written as

$$\begin{aligned} H_{\text{wire}} &= \frac{1}{2} \int dx \Psi(x)^\dagger \left[\left(-\frac{\hbar^2 \partial_x^2}{2m^*} - i\lambda \partial_x \sigma_y - \mu_w \right) \tau_z \right. \\ &\quad \left. + \frac{g\mu_B |B_z|}{2} \sigma_z + \Delta_s \tau_x \right] \Psi(x) \end{aligned} \quad (14)$$

in the Bogoliubov-De Gennes (BdG) formulation. Here we use the Nambu spinor formulation where

$$\Psi(x)^T = (\psi_\uparrow(x), \psi_\downarrow(x), \psi_\downarrow^\dagger(x), -\psi_\uparrow^\dagger(x)) \quad (15)$$

and $\psi_\sigma^\dagger(x)$ and $\psi_\sigma(x)$ are fermionic creation and annihilation field operators. As discussed in Ref. 10, it can be shown that within the limits $|\Delta| < g\mu_B |B_z|/2$ and $g\mu_B |B_z| \gg m^* \lambda^2$ the Hamiltonian in Eq. (14) can be projected to a single-band effective low-energy Hamiltonian that matches Kitaev’s model in Eq. (6). Upon diagonalization, it can be shown that the nanowire Hamiltonian in Eq. (14) can be driven to a topological phase when

$$\frac{g\mu_B |B_z|}{2} > \sqrt{\Delta_s^2 + \mu_w^2}. \quad (16)$$

Experimentally, the chirality of the nanowire can be controlled by strain, which defines the sign of the Rashba spin-orbit coupling in Eq. (14). The direction of the effective electric field due to the strain enters into the spin-orbit Hamiltonian as follows

$$H_{\text{Rashba}} = \frac{g\mu_B}{2mc} (\boldsymbol{\sigma} \times \mathbf{p}) \cdot \mathbf{E}_{\text{eff}}. \quad (17)$$

The interplay between the spin-orbit coupling and the s-wave superconductivity makes the sign of the effective p-wave order parameter directly depends on the relative direction of the strain-induced electric field with respect to a fixed crystal direction [10], namely,

$$\Delta \cong \frac{\lambda \cdot \Delta_s}{g\mu_B B_z} \sim \text{sgn}(\mathbf{E}_{\text{eff}} \cdot \hat{z}). \quad (18)$$

Given the strong connection between the physics encoded in the realistic model represented by Eq. (14) and the Kitaev Hamiltonian in the topological regime, in this paper we adopted the latter for our modeling and analysis of nanowires. This assumption simplifies the calculations without affecting the generality of our conclusions. In Sec. V, we return to the continuum model to connect our results to the experimental parameter space.

B. Electronic tight-binding model of nanowires and junctions

We start by investigating junctions of time-reversal symmetric Kitaev nanowires. We only consider junctions in the

all-connected configuration, where all nanowire endpoints are coupled to each other.

We employ an electronic, single-band electronic tight-binding model based on the Hamiltonian of Eq. (6) to model nanowires and their junctions. We adopt a BdG representation for the fermion operators

$$\psi_{l,\alpha} = \begin{pmatrix} a_{l,\alpha} \\ -a_{l,\alpha}^\dagger \end{pmatrix}, \quad \psi_{l,\alpha}^\dagger = \begin{pmatrix} a_{l,\alpha}^\dagger & -a_{l,\alpha} \end{pmatrix}, \quad (19)$$

where $l = 1, \dots, L$ is the site coordinate and $\alpha = 1, \dots, n$ is the nanowire index. We number the sites by starting from the junction end of the nanowire. The total Hamiltonian of a n -nanowire junction system is written as

$$H_{\text{total}} = \sum_{\alpha=1}^n H_\alpha + H_{\text{junction}}, \quad (20)$$

where

$$H_\alpha = \sum_{l=1}^{L-1} \psi_{l,\alpha}^\dagger (-t \tau_z + i \eta_\alpha |\Delta| \tau_y) \psi_{l+1,\alpha} - \frac{\mu}{2} \sum_{l=1}^L \psi_{l,\alpha}^\dagger \tau_z \psi_{l,\alpha} \quad (21)$$

describes the α -th wire and

$$H_{\text{junction}} = -\frac{1}{2} \sum_{\alpha \neq \beta} \Gamma_{\alpha\beta} \psi_{1,\alpha}^\dagger \tau_z \psi_{1,\beta} \quad (22)$$

describes the couplings at the junction, where $\Gamma_{\alpha\beta}$ is the pairwise hopping amplitude between the endpoints of the α -th and β -th nanowires. For the simulations discussed in this section, we adopt $\mu = 0.5t$, $L = 20$ and $\Delta = 0.5t$, which sets the nanowires in the topological regime and exponentially localize the Majorana zero modes at the nanowire ends, with $\ell_0 \approx 1.82$. We have performed all the numerical simulations in this paper by implementing the tight-binding Hamiltonian of Eq. (20) in Kwant [26].

C. Majorana junctions of 3 wires

We note that for two Majorana zero modes on different time-reversal symmetric nanowires to hybridize and to combine into a finite-energy fermion, they must be of different polarity. This restricts how the zero modes can be distributed among the junction nanowires. In the case of a three-wire junction, two possible cases exist. When all the Majorana zero modes in the junction are of the same polarity, none of the zero modes couple and all six zero modes on the ends of three nanowires survive. However, when one of the nanowires has a different polarity than the other two nanowires, for example, in a $(++-)$ or $(-+-)$ configuration, there is only one zero mode at the junction and the wave function amplitude for that zero mode is shared between the majority polarization sites.

This analysis in terms of Majorana operators is corroborated by a numerical simulation of the underlying electronic

system. The results are presented in Fig. 4, where the electronic local density of states (LDOS) at zero energy for the $(---)$ and $(-+-)$ junction configurations are shown when $\Gamma_{\alpha\beta} = (1 - \delta_{\alpha,\beta})\Gamma$ with $\Gamma = t$. It is clear that for the $(---)$ configuration a total of six Majorana zero modes are present, including three at the junction. For the $(-+-)$ configuration, there is a single zero mode at the junction and it is shared only by the nanowires with majority polarity.

The wave function distribution in the majority-polarized nanowires makes it impossible to satisfy simultaneously the two necessary conditions for the realization of a single-band Majorana network. This is illustrated in Fig. 5 where a brick-wall network out of the nanowires with only one Majorana zero mode at each junction is shown. The Majorana zero mode located on the majority nanowires of a junction is disconnected from the zero mode on the junction across the minority nanowire. As a result, when hybridization within the nanowires is turned on, the network breaks up into an array of disconnected chains with no inter-chain coupling.

D. Majorana junctions of five nanowires

We now consider the case of five nanowires and when $n_+ = 2$ and $n_- = 3$. We simulate such a junction similarly to the three-nanowire junction using the following choice for the $\Gamma_{\alpha\beta}$ coupling parameters:

$$\Gamma_{\alpha\beta} = \frac{\Gamma}{\sqrt{6}} \times \begin{pmatrix} 0 & 0 & 1 & 1 & -2 \\ 0 & 0 & \sqrt{3} & -\sqrt{3} & 0 \\ 1 & \sqrt{3} & 0 & 0 & 0 \\ 1 & -\sqrt{3} & 0 & 0 & 0 \\ -2 & 0 & 0 & 0 & 0 \end{pmatrix}. \quad (23)$$

This choice of coupling matrix elements lifts all by one mode from zero energy. The remaining zero mode has equal amplitude among the three majority-polarity nanowires. The results are shown in Fig. 6. In this case, the single Majorana zero mode wave function is distributed among the negative endpoints of the majority polarization nanowires in the junction, fully connecting the three links of the network that emanate from the junction and condition (i) of Sec. II is satisfied. Moreover, all junction zero modes can be connected to zero modes located at the outer endpoints of the junction nanowires, satisfying condition (ii). This configuration is therefore chosen for the simulation of a ‘‘Majorana graphene’’ network, which we discuss in the following section. While other choices of coupling matrix elements are possible, as long as the diagonal blocks in Eq. (23) are zero, only one zero mode exists at the junction. Small deviations from the coupling matrix elements in Eq. (23) are possible: due to TRS, Dirac cones in the dispersion relation survive as long as the matrix elements satisfy the triangle rule, which says that the magnitude of each of the tunnel couplings is smaller than the sum of the magnitudes of the other two couplings [27]. Moreover, Dirac cones are also robust to inhomogeneities in Γ from one junction to another, as there is no equivalent to on-site disorder in a Majorana ‘‘graphene’’ system.

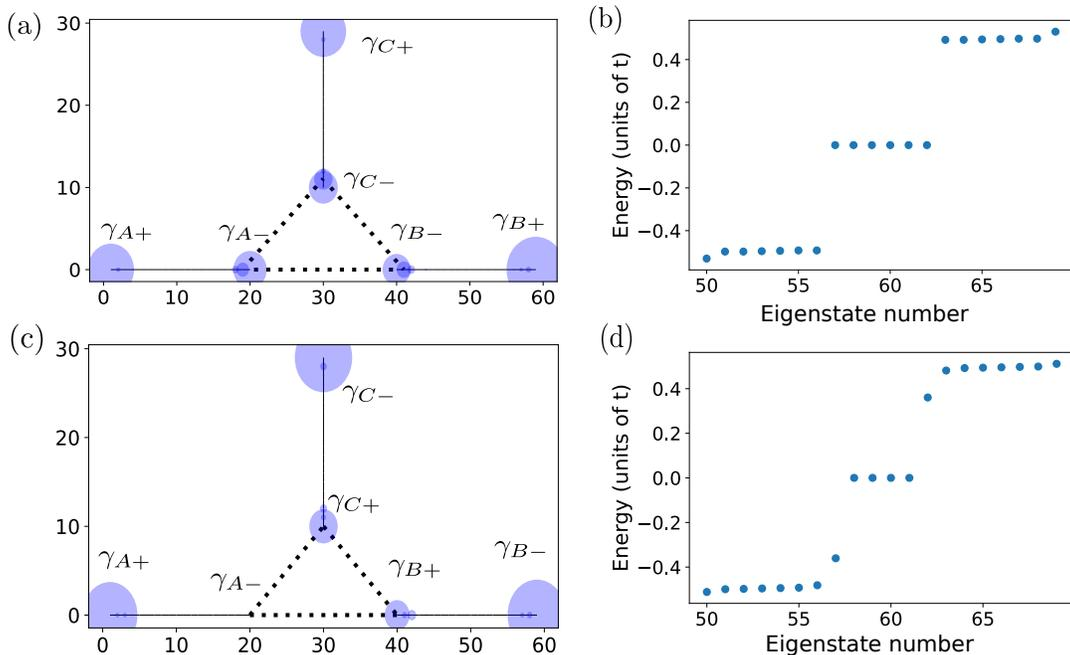


FIG. 4. Numerical results for a three-wire junction with two different choices of polarity. Solid lines indicate the location of the nanowires (site coordinates are shown), while dotted lines connect neighboring nanowire endpoints. To facilitate visualization, neighboring endpoints are set farther apart than one chain lattice constant unit. In panels (a) and (b) the electronic local density of states (LDOS) at zero energy and the energy eigenstates are plotted, respectively, for the $(- - -)$ case, while in panels (c) and (d) the same quantities are plotted for the $(+ + +)$ case. The wires are identified by the subscripts A, B, C . In (a), it is noticeable that the zero-energy wave function has amplitude in the three junction sites and the total number of zero modes is six, with three sitting at the junction and three other modes sitting at the outer ends of the wires. In (c), the zero-energy wave function has amplitude in the majority polarity sites of the junction but there is only zero mode at the junction. The other three modes sit at the outer ends of the nanowires.

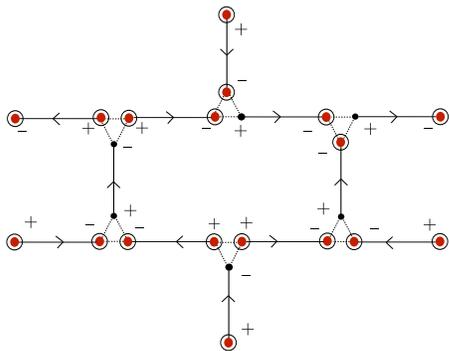


FIG. 5. Schematic illustration of a brickwall network of nanowires with well-defined polarizations and three-wire junctions of the $(- + +)$ and $(+ + -)$ types. The presence of a nonzero Majorana zero mode amplitude at a nanowire end is indicated by a circular line around a solid circle. Nanowire polarities are indicated by arrows and \pm signs.

IV. MAJORANA NETWORK

In Sec. III D, we established that, using a five-wire junction, it is possible to (i) have a single Majorana (quasi-)zero mode per site of the brickwall lattice, and (ii) hybridize this

mode with those on the three neighboring sites. These results justify using the brickwall structure in Fig. 1 to realize the “Majorana graphene” network. Here we proceed to construct the logical Majorana zero mode using this structure, modeling every nanowire in the network by the Kitaev Hamiltonian in the BdG formulation, as in Eq. (21). (In the next section we discuss the connection to a more experimentally realistic model.)

A. “Majorana graphene” network

The characteristic length of the zero modes in the Kitaev nanowires depends on the chemical potential, as indicated in Eq. (7). It is thus possible to increase the overlap between the zero modes in neighboring sites of the network, i.e., effective hopping of the Majorana zero modes in the brickwall lattice, by controlling a gate voltage V_g in every nanowire.

We consider first the case with uniform hopping matrix elements (i.e., uniform gate voltages) across the entire network. In this case, the Majorana system on the brickwall lattice contains features similar to those of graphene, such as a Dirac-type dispersion. To illustrate this point, we computed the electronic energy bands of an infinite honeycomb network of 5-nanowire junctions. In Fig. 7a we show the energy bands close to zero energy, where the six pairs of Dirac cones at

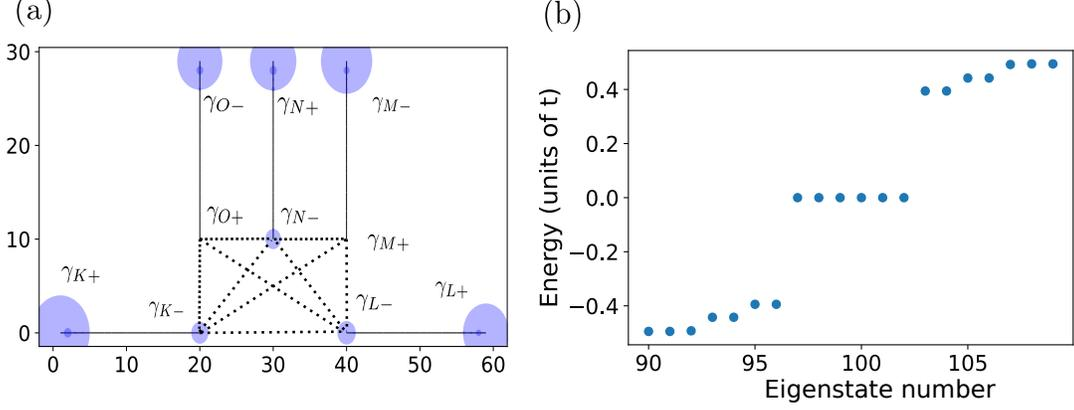


FIG. 6. Numerical results for a five-wire junction consisting of two positive and three negative polarity nanowires coupled according to Eq. (23). The same conventions as in Fig. 4 are followed here. In panel (a), the electronic local density of states (LDOS) at zero energy is plotted while in panel (b) the relevant energy eigenstates are plotted. The wires are identified by the subscripts K, L, M, N, O . It is clear from the electronic LDOS that the zero energy wave function in the junction has nonzero amplitude only in the majority polarity sites. There is no impediment for the zero mode located at a junction can hybridize with the zero modes in neighboring junctions.

the K_{\pm} points are clearly visible. The nanowire parameters are $L = 20$, $\Delta = 0.5t$, and $\mu = 0.5t$; the junction couplings follow Eq. (23), with $\Gamma = t$. In Fig. 7b, we show that the Fermi velocity for the Dirac dispersion depends on the nanowire chemical potential, which in turn controls the effective hopping amplitude between Majorana zero modes located at the opposite ends of the nanowire.

Returning to the finite-size network of Fig. 1 with open boundaries, in Fig. 8 we show its electronic LDOS at zero energy for the network when $\mu = 0.4t$, $\Delta = 0.8t$, and $\Gamma = t$, employing the junction coupling matrix of Eq. (23). The LDOS shows zero energy modes at the boundary and in the bulk of the system. These zero modes correspond to the states at the Dirac nodes (i.e., the apexes of the cones in the energy bands of Fig. 7). Due to the open boundary conditions, zero modes appear at the boundary sites. They can be removed by switching to periodic boundary conditions, as we show in Fig. 9.

B. Kekulé modulation in the brickwall lattice

Introducing a Kekulé dimerization pattern in a graphene lattice opens up a gaps in the Dirac spectrum [1, 21]. The Kekulé modulation can be realized by imposing the following perturbation to the local chemical potential (via gate voltages):

$$\mu = \mu_0 + \delta\mu_{\mathbf{r},\alpha}, \quad (24)$$

where

$$\delta\mu_{\mathbf{r},\alpha}^{\text{Kekule}} = \mu_K \cos(\varphi_{\mathbf{r},\alpha}). \quad (25)$$

and

$$\varphi_{\mathbf{r},\alpha} = \mathbf{K}_+ \cdot \mathbf{s}_{\alpha} + (\mathbf{K}_+ - \mathbf{K}_-) \cdot \mathbf{r}. \quad (26)$$

To implement this modulation, we return momentarily to the equivalent honeycomb lattice and its coordinate system. The position vector \mathbf{r} has a fixed (arbitrary) origin and points to the sites of one of the triangular sublattices. The three vectors s_{α} ($\alpha = x, y, z$) connect sites of that sublattice to their nearest neighbors on the other sublattice. $\mathbf{K}_+ = -\mathbf{K}_-$ are the distinct vectors connecting the Γ to the K points in the reduced Brillouin zone in reciprocal space for the honeycomb lattice. In Fig. 10 we show the pattern induced by the Kekulé distortion.

In Fig. 11, we show the effect resulting from the Kekulé dimerization pattern on the electronic LDOS at zero energy for the wire network in Fig. 1. For these calculations, the junction coupling amplitude $\Gamma = t$, the superconductor order parameter amplitude $\Delta = 0.8t$, and the chemical potential parameters are set as $\mu_0 = t$ and $\mu_K = 0.98t$. We choose the maximum value of the chemical potential ($\mu_{\text{max}} = \mu_0 + \mu_K$) to be very near the boundary of the topological range, $\mu_{\text{max}} = 1.98t < \mu_c = 2t$ to ensure a sizable overlap between the Majorana zero modes on both ends of the same nanowire, with the Majorana characteristic length reaching $\ell_0 \approx 80$ on those nanowires [see Eq. (7)]. Notice that the bulk zero modes are now absent because of the bulk gap, while the boundary zero modes remain. The boundary zero modes disappear under periodic boundary conditions. To illustrate this point, in Fig. 12 we show the energy eigenvalues of a Majorana zero-mode lattice of 4 layers with each layer consists of 5 horizontal wires with periodic boundary conditions in the presence and in the absence of the Kekulé modulation. We adopt the same parameters as in Fig. 8 and Fig. 11. for the absence and presence of Kekulé modulation respectively.

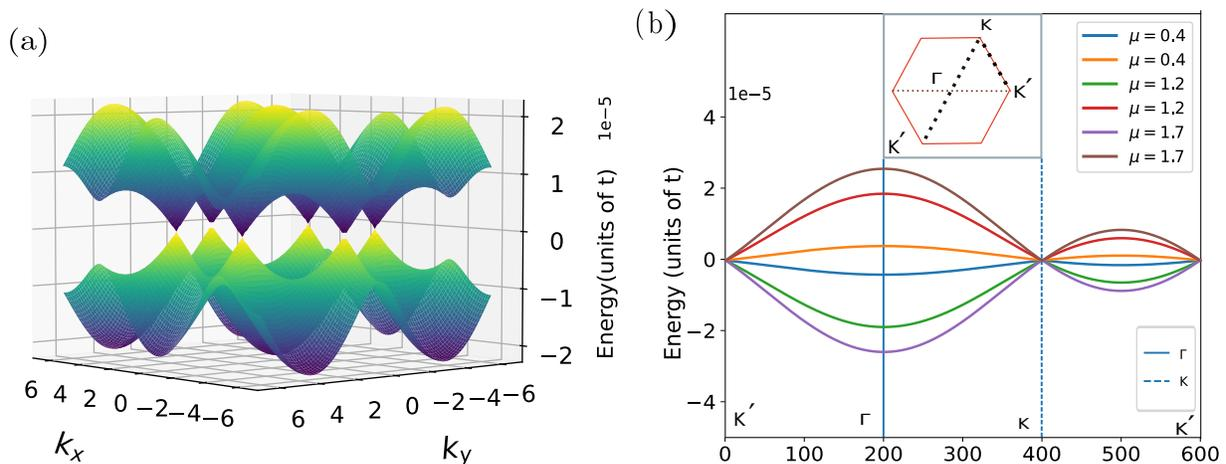


FIG. 7. (a) Electronic energy bands near zero energy for an infinite network of five-wire junctions consisting of two positive and three negative polarity nanowires. The nanowire parameters are $L = 20$, $\Delta = 0.5t$, and $\mu = 0.5t$. The junction coupling parameters are chosen according to Eq. (23) with $\Gamma = t$. The brickwall lattice is reshaped as a honeycomb lattice in order to create a triangular reciprocal lattice unit cell to facilitate visualization of the bands. (b) Energy bands along the reciprocal space dashed line path are shown in the inset. Bands are various chemical potential values are shown to illustrate their impact on the Fermi velocity at the K_{\pm} points.

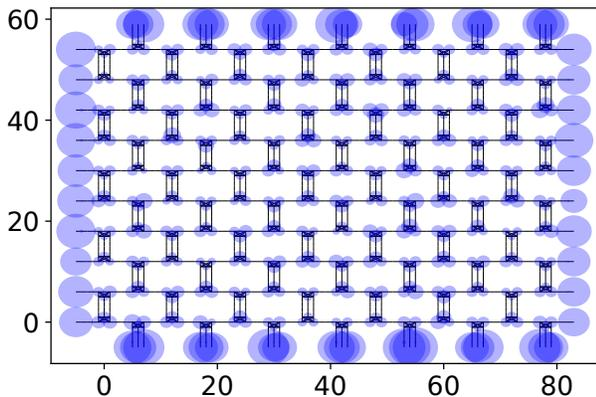


FIG. 8. Electronic LDOS for a 7×10 brickwall lattice of Majorana nanowires with open boundary conditions and a single zero mode at each junction. Horizontal links in the lattice consist of a single nanowire while vertical links contain three wires. Every nanowire is described by a Kitaev chain Hamiltonian with $L = 5$ sites, $\mu = 0.4t$, and $\Delta = 0.8t$. Junction couplings follow Eq. (23) with $\Gamma = t$.

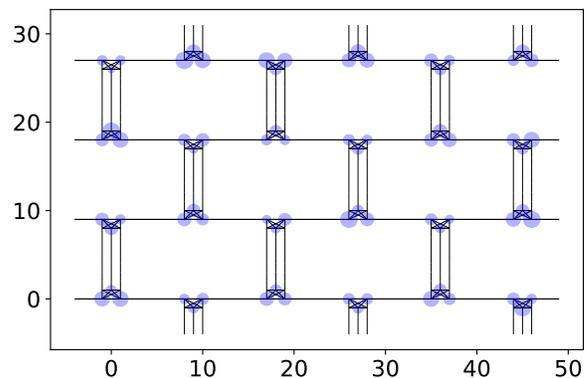


FIG. 9. Electronic LDOS for a 3×4 brickwall lattice of Majorana nanowires similar to that of Fig. 8 but with periodic boundary conditions and $L = 8$. Notice the absence of zero modes at the boundaries. The smaller lattice has been used to show that the boundary Majorana-zero modes disappear when using periodic boundary conditions.

C. Zero modes bound to Kekulé vortices

The Kekulé dimerization pattern can support defects in the form of vortices. As noted in Ref. [1], a vortex can be imprinted via an additional modulation of the Kekulé pattern,

$$\varphi_{\mathbf{r},\alpha} = \mathbf{K}_+ \cdot \mathbf{s}_\alpha + (\mathbf{K}_+ - \mathbf{K}_-) \cdot \mathbf{r} + \varphi_{\mathbf{r}}^{\text{vortex}}, \quad (27)$$

where

$$\varphi_{\mathbf{r}}^{\text{vortex}} = \sum_{n=1}^{\nu} q_n \arg(\mathbf{r} - \mathbf{R}_n). \quad (28)$$

One important advantage of this construction is that the vorticities $q_n = \pm 1$ ($n = 1, \dots, \nu$) and the positions of the vor-

tices \mathbf{R}_n are also programmable via the applied gate voltage on each wire. The Kekulé vortices bind zero energy modes at their location – these are the *logical* Majorana zero mode. These logical Majoranas can be moved by applying gate voltages that correspond to changing the value of \mathbf{R}_n in Eq. (27).

In Fig. 13a,c we show the electronic LDOS at zero energy for the wire network in Fig. 1 with a Kekulé vortex pattern of applied gate voltages. In Fig. 13b,d we plot the intensity of eigenfunctions associated to the zero modes bound to the Kekulé vortex. We choose the vorticity to be -1 . Other parameters are the same as those in Fig. 11

The results described above establish that the wire network presented in Fig. 1 is a concrete realization of the proposal in Ref. [1] to obtain logical Majorana zero modes in a hierar-

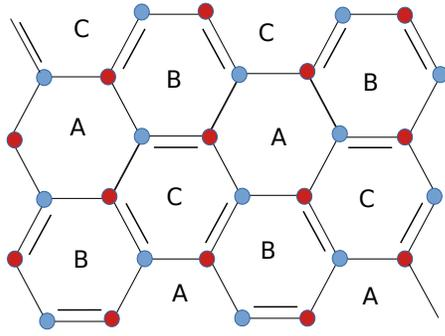


FIG. 10. The Kekulé dimerization in a honeycomb lattice. The single (double) links correspond to weak (strong) bond amplitudes. The red and blue dots represent the two sublattices of the honeycomb lattice. As a result of the dimerization, three kinds of plaquettes are created which are labeled by A, B and C.

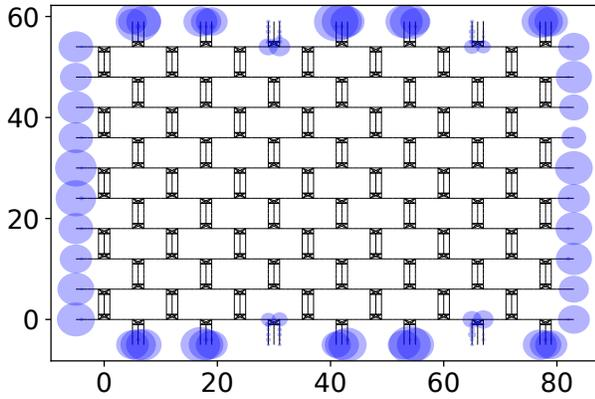


FIG. 11. Electronic LDOS of a brickwall network of Majorana nanowires with a Kekulé distortion on the chemical potentials. Chain and junction parameters are the same as in Fig. 8, with the baseline chemical potential $\mu_0 = t$ and the added Kekulé modulation $\mu_K = 0.98t$.

chical manner. The architecture in Fig. 1 enables the placement of multiple vortices and the movement of those vortices by simply changing the gate voltage on the wires according to Eq. (27). In particular, this construction allows the logical Majorana zero modes to be braided adiabatically by the modulation of the gate voltages.

V. CONNECTION TO EXPERIMENTAL SETUPS

We now connect the idealized tight-binding model used to describe the Majorana network with a more realistic model of semiconductor system proximitized with s-wave superconductors. We return to the Hamiltonian in Eq. (14) and consider an infinite nanowire in the momentum space representation, yielding

$$H_{\text{wire}} = \frac{1}{2} \sum_k \psi_k^\dagger H_k \psi_k, \quad (29)$$

where

$$H_k = (\varepsilon_k + \lambda k \sigma_y - \mu_w) \tau_z + E_Z \sigma_z + \Delta_s \tau_x, \quad (30)$$

$\varepsilon_k = \hbar^2 k^2 / 2m^*$, and $E_Z = g\mu_B |B|/2$. The eigenvalues of this matrix are

$$E_k = \pm \sqrt{(\varepsilon_k - \mu)^2 + E_Z^2 + \Delta_s^2 + \lambda^2 k^2 \pm 2R_k}, \quad (31)$$

where

$$R_k = \sqrt{(\varepsilon_k - \mu)^2 (E_Z^2 + \lambda^2 k^2) + \Delta_s^2 E_Z^2}. \quad (32)$$

Each one of the four eigenvalues generates a band in k -space. The exact shape of these bands depends sensitively on the values of the parameters m^* , E_Z , Δ_s , λ , and μ_w . Therefore, it is fundamental to seek parameter values that match experimental systems. For that purpose, we choose InSb-NbTiN hybrid nanowires, which are currently used to realize Majorana zero modes. They have a proximity-effect induced superconductor gap $\Delta \approx 1$ meV. The effective mass of bulk InSb is $m^* = 0.014 m_e$, where m_e is the electron bare mass [28]. The Rashba spin-orbit coupling parameter for bulk InSb is $\lambda = 0.1$ eV·nm and the g-factor is 50 [29]. Since it is advantageous to use a large magnetic field and the critical field for bulk NbTiN is approximately 10 T, we pick this value for our analysis. Thus, following Eq. (16), the range of chemical potential values for which the nanowire remains in the topological phase is $|\mu_w| \lesssim 11$ meV.

After substituting those experimental parameter values into Eq. (31) we find low-lying energy bands which can we well approximated by the dispersion relation

$$E_k \approx \sqrt{\alpha(k \pm k_0)^2 + \beta}, \quad (33)$$

with $\alpha \approx 0.140$ eV²·nm², $k_0 \approx 0.0777$ eV²·nm, and $\beta \approx 2.23 \times 10^{-7}$ eV².

We can similarly derive a low-lying band structure from the Kitaev chain Hamiltonian in Eq. (13). In the long wave-length limit, we find an expression that matches Eq. (33), allowing us to connect its coefficients with the Kitaev chain parameters as follows:

$$t a^2 = \frac{\sqrt{\alpha}}{k_0}, \quad (34)$$

$$t - \frac{\mu}{2} - \frac{\Delta^2}{t} = \frac{\sqrt{\alpha} k_0}{2}, \quad (35)$$

and

$$\beta = \frac{\Delta^2}{2t} \left[2t - \mu - \frac{2\Delta^2}{t} \right], \quad (36)$$

where a is the chain lattice constant. These relations are obtained under the assumption that $\mu < 2t - \Delta^2/t$. Inserting the experimental values for α , k_0 , and β into these relations, we find that a realistic Kitaev model parameters satisfy

$$t a^2 \approx 4.8 \text{ eV} \cdot \text{nm}^2 \quad (37)$$

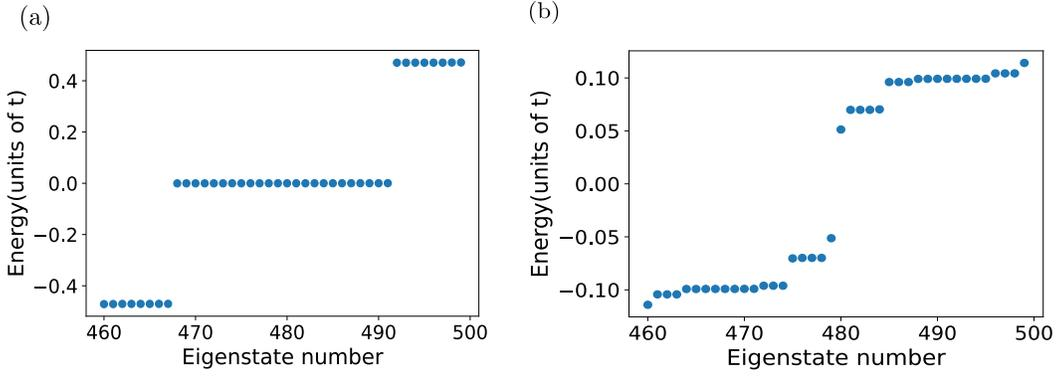


FIG. 12. The energy spectrum of a brickwall lattice with quasi-Majorana zero modes at each vertex and periodic boundary conditions without (a) and with (b) a Kekulé modulation for $L = 8$ and the same network size as in Fig. 9. The parameters used in panels (a) and (b) are the same as those in Fig. 8 and Fig. 11, respectively.

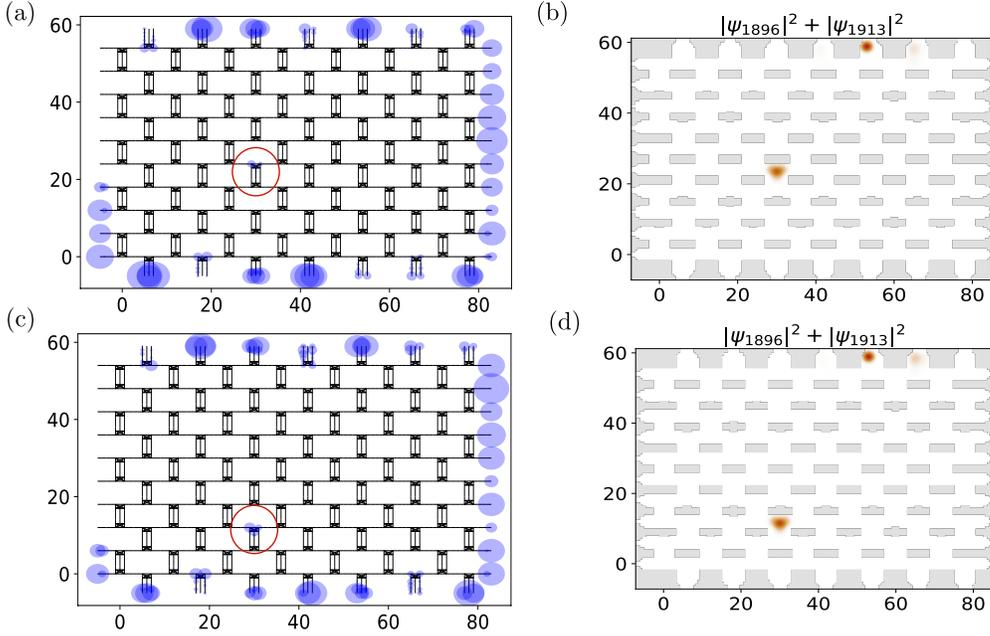


FIG. 13. Vortex in a Majorana network. The electronic LDOS at zero energy is plotted in panels (a) and (c) for the two different vortex positions indicated by red circles. The intensity of the eigenstates located within the red circles is plotted in panels (b) and (d). Notice that the eigenstate are the same for both vortex positions. The Majorana zero modes in the bulk are bound to the Kekulé vortex and they move around lattice together with the vortex. The location of the vortex is controlled by gate voltages on the nanowires. Here the vortex has charge $q = -1$. All other parameters are the same as in Fig. 8.

and

$$t - \frac{\mu}{2} - \frac{\Delta^2}{t} = 0.015 \text{ eV}. \quad (38)$$

Let us consider the case when $\Delta = 0.5t$ and $\mu = 0.5t$, corresponding to the regime of Figs. 4 and 6. Substituting these values into the above equations we find $t = 7.3 \text{ meV}$ and $a = 26 \text{ nm}$; the latter value, when combined with a length of 20 sites ($L = 20$) yields a wire of approximately 500 nm in length, which is quite reasonable when considering a realistic nanowire. Equation (36) serves as a consistency check: The r.h.s. yields 1 meV, which is about 5 times larger than the fit-

ted value for β . This discrepancy comes primarily from Δ , which is set to a relatively high value in the numerical calculations to keep the Majorana zero modes sufficiently isolated at the ends of the chains. Smaller values of Δ could be implemented at the expense of using longer chains (i.e., more sites) and performing exact diagonalizing of larger systems. However, given that the values obtained for a and t in comparison to the realistic nanowire model are reasonable, and they dependent only weakly on Δ when $\Delta \ll t$, our considerations show that it is possible to achieve the necessary conditions for the realization of Majorana zero modes in current experimen-

tal setups.

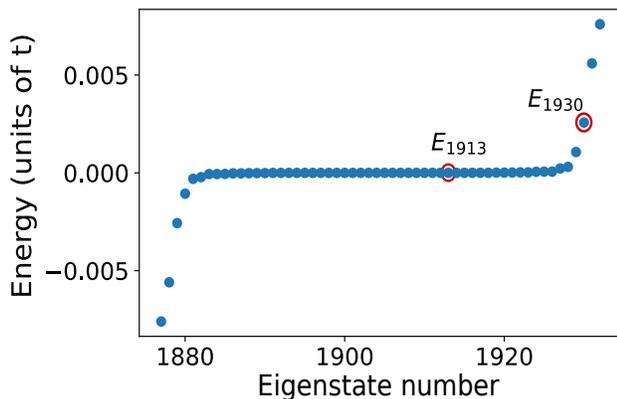


FIG. 14. Energy eigenstates for the brickwall lattice in the presence of a vortex. The E_{1913} eigenstate along with its particle-hole partner is the vortex eigenstate. The closest state which does not contribute to the boundary zero modes is the state E_{1930} .

Another important aspect to consider in connection to the experimental observation of Majorana zero modes is the necessary energy resolution. In Fig. 14, we show a portion of the energy spectrum for the brickwall lattice for the specific vortex position in Fig. 13a. We notice that the difference in energy between the nearest bulk zero mode state is $0.00257t$. Using the value of t obtained from the fitting to the realistic nanowire model, this energy separation equals approximately $19 \mu\text{eV}$, or, equivalently, 220 mK , which is a very accessible temperature.

VI. SUMMARY

In this work we present a nanowire architecture, shown in Fig. 1, where it is possible to realize logical Majorana zero modes that are movable in 2D by changing gate voltages on the nanowires. This architecture realizes the hierarchical construction of Ref. [1], without the need for breaking time-reversal symmetry (TRS).

The basis for building the logical Majorana zero modes is a programmable ‘‘Majorana graphene’’ platform, where a single Majorana quasi-zero mode at each site of a brickwall or of a honeycomb lattice hybridizes with modes on the three neighboring sites. The degree of hybridization, and hence the

effective hopping, is controlled by gate voltages. To arrive at the geometry in Fig. 1, we showed that junctions of five nanowires meeting at each site are necessary so that (i) there is a single (quasi-)zero mode in each site; and (ii) this single mode hybridizes with the three neighboring sites. The number of nanowires needed at the junction follows from two indices constructed from the polarities of the zero modes at the end of nanowires. (A positive polarity corresponds to zero modes that are even under TRS, while a negative polarity corresponds to modes that are odd under TRS.) For a junction where n_+ positive and n_- negative polarities meet, the number of zero modes at the junction is $\nu = |n_+ - n_-|$ and the wave function of the zero modes spread over $\rho = \max(n_+, n_-)$ wires. We thus satisfy conditions (i) and (ii) with either $n_+ = 3$ and $n_- = 2$, or $n_+ = 2$ and $n_- = 3$, which are the cases in the two sublattices of the brickwall network shown in Fig. 1. In the paper, we show numerical results obtained from electronic tight-binding models of nanowire junctions are in agreement with this counting.

We further carried out numerical studies of a tight-binding model for all nanowires and junctions of the network in Fig. 1. In particular, we decorated the tight-binding model with a Kekulé dimerization pattern and showed that it is possible to make the bulk of the system gapped. We achieved the final stage in the hierarchical construction of Ref. [1] by including vortices in the Kekulé dimerization pattern and showed that there exists a zero mode – the logical Majorana mode – at the core of the Kekulé vortex. Finally, we provided estimates of the experimental values for the parameters used in the numerical calculations and argued that it is possible to detect the logical Majorana zero modes using low-temperature local probes.

In closing, we stress that the construction of movable logical Majorana zero modes in 2D would enable direct and controllable experiments where Majoranas are braided. This realization of braiding may require less stringent conditions on the nanowires than other proposals in the literature.

ACKNOWLEDGMENTS

The authors would like to thank Hongji Yu for valuable discussions at the early stages of this work. This work was partially supported by the U.S. Department of Energy, Office of Science, Basic Energy Sciences, under Award DE-SC0019275, and by NSF Grant DMR-1906325 (C.C. and G.G.).

-
- [1] Z.-C. Yang, T. Iadecola, C. Chamon, and C. Mudry, *Phys. Rev. B* **99**, 155138 (2019).
 [2] E. Dennis, A. Kitaev, A. Landahl, and J. Preskill, *J. Math. Phys.* **43**, 4452 (2002).
 [3] S. B. Bravyi and A. Y. Kitaev, *Quantum codes on a lattice with boundary* (1998), [arXiv:quant-ph/9811052](https://arxiv.org/abs/quant-ph/9811052).
 [4] A. G. Fowler, M. Mariantoni, J. M. Martinis, and A. N. Cleland,

- Phys. Rev. A* **86**, 032324 (2012).
 [5] A. Y. Kitaev, *Annals of Physics* **303**, 2 (2003).
 [6] C. Nayak, S. H. Simon, A. Stern, M. Freedman, and S. Das Sarma, *Rev. Mod. Phys.* **80**, 1083 (2008).
 [7] A. Kitaev, *Annals of Physics January Special Issue*, **321**, 2 (2006).
 [8] A. Y. Kitaev, *Phys.-Usp.* **44**, 131 (2001).

- [9] L. Fu and C. L. Kane, *Phys. Rev. Lett.* **100**, 096407 (2008).
- [10] J. Alicea, Y. Oreg, G. Refael, F. von Oppen, and M. P. A. Fisher, *Nature Phys* **7**, 412 (2011).
- [11] S. Fujimoto, *Phys. Rev. B* **77**, 220501 (2008).
- [12] R. M. Lutchyn, J. D. Sau, and S. Das Sarma, *Phys. Rev. Lett.* **105**, 077001 (2010).
- [13] J. Alicea, *Phys. Rev. B* **81**, 125318 (2010).
- [14] Y. Oreg, G. Refael, and F. von Oppen, *Phys. Rev. Lett.* **105**, 177002 (2010).
- [15] V. Mourik, K. Zuo, S. M. Frolov, S. R. Plissard, E. P. A. M. Bakkers, and L. P. Kouwenhoven, *Science* **336**, 1003 (2012).
- [16] R. M. Lutchyn, T. D. Stanescu, and S. Das Sarma, *Phys. Rev. Lett.* **106**, 127001 (2011).
- [17] J. D. Sau, R. M. Lutchyn, S. Tewari, and S. Das Sarma, *Phys. Rev. Lett.* **104**, 040502 (2010).
- [18] M. Aghaee, A. Akkala, Z. Alam, R. Ali, A. A. Ramirez, M. Andrzejcuk, A. E. Antipov, P. Aseev, M. Astafev, B. Bauer, J. Becker, S. Boddapati, F. Boekhout, J. Bommer, E. B. Hansen, T. Bosma, L. Bourdet, S. Boutin, P. Caroff, L. Casparis, M. Cassidy, A. W. Christensen, N. Clay, W. S. Cole, F. Corsetti, A. Cui, P. Dalampiras, A. Dokania, G. de Lange, M. de Moor, J. C. E. Saldaña, S. Fallahi, Z. H. Fathabad, J. Gamble, G. Gardner, D. Govender, F. Griggio, R. Grigoryan, S. Gronin, J. Gukelberger, S. Heedt, J. H. Zamorano, S. Ho, U. L. Holgaard, W. H. P. Nielsen, H. Ingerslev, P. J. Krogstrup, L. Johansson, J. Jones, R. Kallaher, F. Karimi, T. Karzig, C. King, M. E. Kloster, C. Knapp, D. Kocon, J. Koski, P. Kostamo, M. Kumar, T. Laeven, T. Larsen, K. Li, T. Lindemann, J. Love, R. Lutchyn, M. Manfra, E. Memisevic, C. Nayak, B. Nijholt, M. H. Madsen, S. Markussen, E. Martinez, R. McNeil, A. Mullally, J. Nielsen, A. Nurmohamed, E. O'Farrell, K. Otani, S. Pauka, K. Petersson, L. Petit, D. Pikulin, F. Preiss, M. Q. Perez, K. Rasmussen, M. Rajpalke, D. Razmadze, O. Reentila, D. Reilly, R. Rouse, I. Sadovskyy, L. Sainiemi, S. Schreppler, V. Sidorkin, A. Singh, S. Singh, S. Sinha, P. Sohr, T. Stankevič, L. Stek, H. Suominen, J. Suter, V. Svidenko, S. Teicher, M. Temuerhan, N. Thiagarajah, R. Tholapi, M. Thomas, E. Toomey, S. Upadhyay, I. Urban, S. Vaitiekėnas, K. Van Hoogdalem, D. V. Viazmitinov, S. Waddy, D. Van Woerkom, D. Vogel, J. Watson, J. Weston, G. W. Winkler, C. K. Yang, S. Yau, D. Yi, E. Yucelen, A. Webster, R. Zeisel, and R. Zhao, *InAs-Al Hybrid Devices Passing the Topological Gap Protocol* (2022), arXiv:2207.02472 [cond-mat].
- [19] C.-X. Liu, J. D. Sau, T. D. Stanescu, and S. Das Sarma, *Phys. Rev. B* **96**, 075161 (2017).
- [20] J. A. Sauls, *Philosophical Transactions of the Royal Society A: Mathematical, Physical and Engineering Sciences* **376**, 20180140 (2018).
- [21] C. Chamon, *Phys. Rev. B* **62**, 2806 (2000).
- [22] C.-Y. Hou, C. Chamon, and C. Mudry, *Phys. Rev. Lett.* **98**, 186809 (2007).
- [23] S. Ryu, C. Mudry, C.-Y. Hou, and C. Chamon, *Phys. Rev. B* **80**, 205319 (2009).
- [24] A. P. Schnyder, S. Ryu, A. Furusaki, and A. W. W. Ludwig, *Phys. Rev. B* **78**, 195125 (2008).
- [25] L. Fidkowski and A. Kitaev, *Phys. Rev. B* **81**, 134509 (2010).
- [26] C. W. Groth, M. Wimmer, A. R. Akhmerov, and X. Waintal, *New J. Phys.* **16**, 063065 (2014).
- [27] A. Bernevig and T. L. Hughes, *Topological Insulators and Topological Superconductors* (Princeton University Press, Princeton, 2013).
- [28] H. A. Nilsson, P. Caroff, C. Thelander, M. Larsson, J. B. Wagner, L. E. Wernersson, L. Samuelson, and H. Q. Xu, *Nano Letters* **9**, 3151 (2009).
- [29] R. M. Lutchyn, E. P. a. M. Bakkers, L. P. Kouwenhoven, P. Krogstrup, C. M. Marcus, and Y. Oreg, *Nat Rev Mater* **3**, 52 (2018).